Iron(II) complexes with polydentate Schiff base ligands as models of the photosynthetic mononuclear non-heme ferrous sites. Synthesis, characterization, molecular crystal structure, EXAFS and XANES studies, Mössbauer spectroscopy and magnetic properties

Andriamirado Rakotonandrasana, Didier Boinnard, Jean-Michel Savariault, Jean-Pierre Tuchagues*

Laboratoire de Chimie de Coordination du CNRS (Unité no. 8241, liée par Conventions à l'Université Paul-Sabatier et à l'Institut National Polytechnique), 205 route de Narbonne, 31077 Toulouse Cédex (France)

Vasili Petrouleas

Nuclear Research Center 'Demokritos', 15310 Aghia Paraskevi, Athens (Greece)

Christophe Cartier and **Michel Verdaguer**

Laboratoire de Chimie Inorganique and Laboratoire d'Utilisation du Rayonnement Electromagnétique, Université de Paris-Sud, 91405 Orsay Cédex (France)

(Received June 6, 1990)

Abstract

A series of four high-spin ferrous complexes of polydentate Schiff base ligands has been prepared and studied with IR, X-ray absorption and Mössbauer spectroscopy and variable-temperature magnetic susceptibility. The ligands include potentially tridentate and hexadentate Schiff bases with N_2O and N_4O_2 donor sets, respectively, and result from the condensation of 5-nitrosalicylaldehyde with 2-(aminoethyl)pyridine or tetramines. The results obtained provide evidence that the four complexes described herein are mononuclear high-spin iron(II) species at room temperature. The crystal and molecular structure of $[Fe(5NO_2\text{-salaep})_2]$ (**1**) has been determined. **1** crystallizes in the orthorhombic system, space group *Pbcn* with $Z=4$ and $a=14.756(3)$, $b=9.682(3)$, $c=18.632(4)$ Å. The structure was solved by the heavy-atom method and refined to conventional agreement indices $R=0.042$ and $R_w=0.043$ with 2845 unique reflections for which $I>3\sigma$. The structure of **1** consists of $[Fe(5NO_2\text{-salaep})_2]$ complex molecules stacked through π interactions involving the salicylaldimine rings of adjacent molecules to afford ribbons along the [001] direction. The central iron atom of each molecule is triply coordinated to two $5NO_2$-salaep ligands, affording a distorted coordination octahedron. The Mössbauer spectroscopy is consistent with an increase of the distortion of the iron(II) ligand environment in the series from $[Fe^{II}(5NO_2\text{-salaep})_2]$ (**1**) to $Fe^{II}[5NO_2\text{-sal-N}(1,5,9,13)]$ (**4**). The variable temperature magnetic susceptibility evidences appreciable zero-field splitting of the iron(II) ground state in $[Fe^{II}(5NO_2\text{-salaep})_2]$ (**1**) and $Fe^{II}[5NO_2\text{-sal-N}(1,5,8,12)]$ (**3**). **1** exhibits several properties required to afford a modelling of the iron center of the 'ferroquinone complex' of photosystem 2. $Fe^{II}[5NO_2\text{-sal-N}(1,4,7,10)]$ (**2**) exhibits a thermally induced $^5T_{2g} \leftrightarrow {}^1A_{1g}$ spin conversion with unprecedented features: iron(II) center in a N_4O_2 ligand environment, spin conversion of discontinuous nature occurring in two steps separated by a 30 K broad spin equilibrium domain in which *c.* 50% of high-spin and low-spin molecules coexist.

Introduction

An iron(II) protein complex is located nearby the primary (Q_A) and secondary (Q_B) quinone electron acceptors of photosystem 2 and bacterial reaction centers. Recent X-ray structural studies of crystallized bacterial reaction centers [1] show that the iron atom is located *c.* 7 Å apart from each quinone and directly bonded to four nitrogen atoms pertaining to histidine imidazoles and two oxygen atoms from a carboxylic group pertaining to a glutamic acid residue of the surrounding protein. Based on spectroscopic studies and sequence homologies, a similar arrangement is believed to be present in photosystem 2. Differences, however, exist in the redox potential of the iron(II) (lower in photosystem 2) [2] and the presence of replaceable ligands in the later [2a]. These differences are attributed to the presence of CO_2/HCO_3 as an

*Author to whom correspondence should be addressed.

0020-1693/91/$3.50

axial ligand in photosystem 2 [2a] in place of the glutamic acid residue evidenced in bacteria.

Despite the geometrical position of the iron(II) atom and recent evidence indicating that electron pathways exist from Q_A^- to Fe(III) [2] and from Fe(II) to Q_B^- in photosystem 2 [3, 4], no evidence exists supporting valence state changes of Fe(II), either in bacteria or in photosystem 2, during normal electron flow from Q_A to Q_B. The role of the iron remains poorly understood so far. The electronic structure of Fe(II) is not well resolved yet. Although crystal field simulations of the magnetic properties [5] and weak interaction with Q_A^- in the bacterial case [6, 7] have been worked out, no single set of parameters exists which can explain all existing data including the quadrupole splitting variation and the unusually small broadening of the Mössbauer spectra in the presence of applied magnetic fields [8, 9].

We present in this paper the study of iron(II) complexes with N_4O_2 donor sets aimed at modelling the immediate environment of the photosynthetic iron. These investigations may be proven more broadly applicable since the iron(II) in 4,5-dioxygenase has Mössbauer properties remarkably similar to those of the bacterial iron(II) [10] and the EPR spectra of the oxidized iron of photosystem 2 [2, 4] have strong similarities with those of a number of oxygenases [10, 11].

The four iron(II) complexes studied herein include either two tridentate Schiff base ligands, $5NO_2$-salaep, each affording a N_2O donor set, or one hexadentate Schiff base ligand, $5NO_2$-sal-N(v,w,x,y), affording a N_4O_2 donor set (Fig. 1). The synthesis and IR and Mössbauer spectroscopy and variable temperature magnetic susceptibility for these four complexes are reported and discussed based on the X-ray crystal structure determination of [Fe(5-NO_2salaep)$_2$] (**1**) and EXAFS and XANES studies of all four compounds.

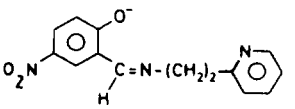

5-NO_2-salaep

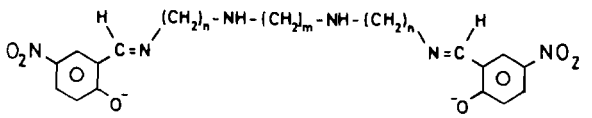

n	m	ligand
2	2	5-NO_2-sal-N(1,4,7,10)
2	3	5-NO_2-sal-N(1,5,8,12)
3	3	5-NO_2-sal-N(1,5,9,13)

Fig. 1. Schematic representation and abbreviation of the ligands.

Experimental

Materials

1,4,7,10-Tetraazadecane(N-1,4,7,10) was purchased from Fluka in high purity grade and used as received. 1,5,8,12-Tetraazadodecane (Strem) and 2-(aminoethyl)pyridine (Aldrich) were fractionally distilled at 118 °C (0.2 mm Hg) and 93 °C (760 mm Hg), respectively. 5-Nitrosalicylaldehyde (Eastman) was sublimed prior to use. 1,5,9,13-Tetraazatridecane was prepared as previously described [12]. Iron acetate tetrahydrate was prepared in a Schlenk vessel under an atmosphere of purified nitrogen [12] according to literature methods [13] and stored in an inert atmosphere box (Vacuum Atmospheres H.E.43.2) equipped with a dry-train (Jahan EVAC7). Methanol was distilled under nitrogen and degassed under vacuum prior to use.

Ligands

$5NO_2$-salaep resulted from the Schiff base condensation of equimolar quantities of 5-nitrosalicylaldehyde ($5NO_2$-sal) and 2-(aminoethyl)pyridine (aep). The ligands $5NO_2$-sal-N(v,w,x,y) resulted from the Schiff base condensation of 5-nitrosalicylaldehyde with the desired tetramine (N-(1,4,7,10) or N-(1,5,8,12) or N-(1,5,9,13)) in the 2:1 ratio. The ligands were obtained as yellow-to-orange microcrystalline powders as previously described [12].

Complexes

Due to the oxygen sensitivity of the starting iron(II) acetate, all reactions were performed under an atmosphere of purified nitrogen by using Schlenk techniques. The general method of preparation was adapted from that described for the parent manganese(II) complexes [12]. The analytical results for the complexes are in good agreement with the theoretical values for C, H, N and Fe. *Anal.* Fe(5-NO_2-salaep)$_2$·MeOH (**1**): C, 55.24 (55.43); H, 4.18 (4.49); N, 12.83 (13.37); Fe, 9.35 (8.89)%. Fe(5-NO_2-sal-N(1,4,7,10))·MeOH (**2**): C, 47.69 (47.56); H, 4.57 (4.94); N, 15.82 (15.85); Fe, 10.28 (10.53)%. Fe(5-NO_2-sal-N(1,5,8,12))·MeOH (**3**): C, 49.21 (49.47); H, 5.00 (5.41); N, 14.70 (15.05); Fe, 10.16 (10.00)%. Fe(5-NO_2-sal-N(1,5,9,13))·0.5MeOH (**4**): C, 49.91 (50.73); H, 4.99 (5.43); N, 15.00 (15.10); Fe, 9.80 (10.04)%.

Physical measurements

Element analyses were carried out at the microanalytical laboratory of the Laboratoire de Chimie de Coordination for C, H and N, and at the Service Central de Microanalyses du CNRS in Vernaison for Fe. IR spectra were recorded on a Perkin-Elmer 983 spectrophotometer coupled with a Perkin-Elmer infrared data station. Samples were run as CsBr pellets prepared under nitrogen in the dry-box.

Variable temperature magnetic susceptibility data were obtained as previously described [14] on polycrystalline and vaseline paste samples with a Faraday type magnetometer equipped with a continuous flow Oxford Instruments cryostat.

Mössbauer measurements were obtained with a constant acceleration conventional spectrometer and a ^{57}Co(Rh) source. Computer simulations were obtained with a least-squares fitting program assuming independent Lorentzian lines. Isomer shift values throughout the paper are given with respect to metallic iron at room temperature.

The X-ray absorption spectra were recorded at LURE on the EXAFS III spectrometer of the DCI storage ring with a two-crystals monochromator (Si 311, 2 mm entrance slit for EXAFS, 0.5 mm entrance slit for XANES) with a storage ring energy of 1.85 GeV and a mean intensity of 150 mA* The monochromator was slightly detuned to insure harmonics rejection. Gas-filled ionization chambers were used to measure the flux intensity including a helium–neon mixture and air for the first (I_0) and second (I) chambers, respectively.

The XANES spectra were recorded step by step, every 0.25 eV with a one second accumulation time per point. The spectrum of a 5 μm iron foil was recorded just after or before an unknown XANES spectrum to check the energy calibration, thus insuring an energy accuracy of 0.25 eV. The EXAFS spectra were recorded in the same way over 1000 eV, with 2 eV steps and one second accumulation time per point. The experiments were calibrated by using the 8991.1 eV peak at the top of the edge of a metallic foil of copper and verifying that the first inflexion point in the spectrum of the iron foil was 7111.2 eV.

Samples were well pounded microcrystalline powders of homogeneous thickness and calculated weight, compressed between two X-ray transparent windows. The absorbance jump at the edge was typically one.

*Abbreviations: DCI, Dispositif de Collision dans l'Igloo; EXAFS, extended X-ray absorption fine structure; LURE, Laboratoire d'Utilisation du Rayonnement Electromagnétique; XANES, X-ray absorption near edge structure; XRD, X-ray diffraction.

The XANES spectra were analyzed following a traditional method. A linear background, determined by least-squares fitting of the pre-edge experimental points was substracted from the experimental spectrum. The spectra were normalized by taking the EXAFS background extrapolation as unit absorbance. The energy of the pre-edge transition was determined by fitting the experimental curves with polynomial functions and taking the first and the second derivatives. The EXAFS analysis followed the method already described [15, 16] and used the EXAFS chain of programs written by Michalowicz either on a UNIVAC or MACINTOSH microcomputer [17] associated with the MINUIT function minimization program [18] and Teo and Lee tabulated amplitude and phase shifts [19].

X-ray crystal structure determination of [Fe(5NO$_2$-salaep)$_2$] (1)

Crystals of complex **1** were obtained inside the inert-atmosphere box by slow interdiffusion of solutions of the 5NO$_2$-salaep ligand and of ferrous acetate in methanol. They were free of methanol solvate molecules. These crystals belong to the orthorhombic system, space group *Pbcn* (D_{2h}, No. 14). The selected crystal was a black parallelipiped of approximate dimensions $0.5\times0.2\times0.3$ mm. It was sealed on a glass fiber and mounted on an Enraf-Nonius CAD 4 diffractometer. Cell constants were obtained from a least-squares fit of 25 reflections. Crystal and intensity collection data are summarized in Table 1. A total of 9008 reflections was recorded to a 2θ(Mo) maximum of 80° by procedures described elsewhere [20]. Intensity standards, recorded periodically, showed no significant variations during measurements. Reflections were corrected for Lorentz and polarization effects [21], 2845 of which with $I>3\sigma$ were used in subsequent calculations. Empirical absorption corrections were made.

Structure solution and refinement

The structure was solved by using the heavy-atom method [22]. The iron atom lying on a *C*2 axis, the refinement has been carried out with half a molecule. A succession of difference Fourier syntheses and least-squares refinements revealed the positions of all atoms including the hydrogen ones. All non-hydrogen atoms were refined anisotropically. All hydrogen atoms were included in the calculations using idealized positions (C–H = 0.97 Å) and afforded a mean isotropic temperature factor $U=0.051(3)$ Å^2. The atomic scattering factors used were those proposed by Cromer and Waber [23] with anomalous dispersion effects [24]. The final full-matrix least-squares refinement, minimizing

TABLE 1. Crystallographic data for [Fe(5NO$_2$-salaep)$_2$] (1)

Formula of the assymmetric unit	$C_{28}H_{24}N_6O_6Fe$
Formula weight	596.38
a (Å)	14.756(3)
b (Å)	9.682(3)
c (Å)	18.632(4)
V (Å^3)	2662(1)
Space group	$Pbcn$ (D_{2h}, No. 14)
Z	4
D_{obs} (g cm^{-3})	1.49(2)
D_{calc} (g cm^{-3})	1.49
Temperature (K)	295
Radiation	Mo Kα, λ=0.71069 Å, graphite monochromator
μ(Mo Kα) (cm^{-1})	6.17
$R=\Sigma\|k\|F_o\|-\|F_c\|\|/\Sigma k\|F_o\|$	0.042
$R_w=[\Sigma w(k\|F_o\|-\|F_c\|)^2/\Sigma wk^2F_o^2]^{1/2}$	0.043

$\Sigma w(|F_o|-|F_c|)^2$ converged to $R=\Sigma||F_o|-|F_c||/\Sigma|F_o|=0.042$ and $R_w=[\Sigma w(|F_o|-|F_c|)^2/\Sigma w|F_o|^2]^{1/2}=0.043$ with a weighting scheme $w=1$. The goodness of fit was $s=1.24$ with 2845 observations and 187 variables.

All calculations were performed on a VAX 11/730 DEC computer using the programs SDP [21], SHELX 76 [25], SHELX 86 [22] and ORTEP [26]. The [Fe(5NO$_2$-salaep)$_2$] molecule is shown in Fig. 2 with atom numbering. Final fractional atomic coordinates with their estimated standard deviations and bond lengths and angles are given in Tables 2 and 3, respectively. See also 'Supplementary material'.

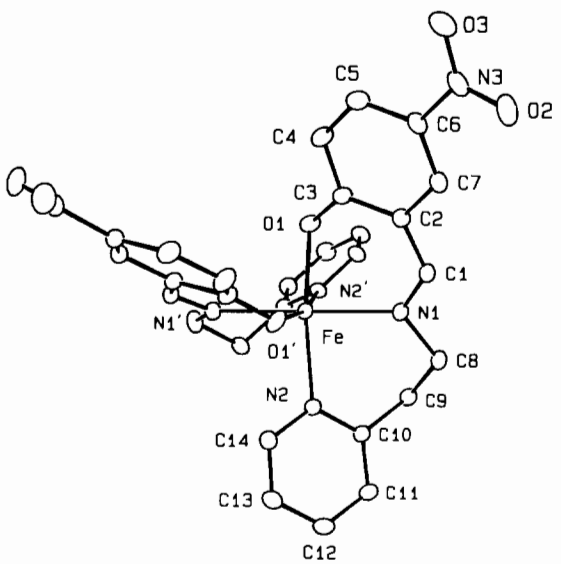

Fig. 2. ORTEP view of the [Fe(5NO$_2$-salaep)$_2$] molecule (1).

TABLE 2. Fractional atomic coordinates and isotropic thermal parameters of non-hydrogen atoms for [Fe(5NO$_2$-salaep)$_2$] (1) with e.s.d.s in parentheses

Atom	x/a	y/b	z/c	U_{iso}
Fe	0.00000(0)	0.14019(5)	0.25000(0)	3.12(6)
O(1)	−0.0634(1)	0.2945(2)	0.1932(1)	4.3(3)
N(2)	0.0944(1)	−0.0065(2)	0.3036(1)	3.4(3)
N(1)	0.0966(1)	0.1386(2)	0.1612(1)	3.6(3)
C(1)	0.1113(2)	0.2453(3)	0.1223(1)	3.7(4)
C(2)	0.0607(2)	0.3731(3)	0.1214(1)	3.5(4)
C(3)	−0.0252(2)	0.3903(3)	0.1572(2)	3.5(4)
C(4)	−0.0685(2)	0.5217(3)	0.1495(2)	4.8(5)
C(5)	−0.0316(2)	0.6255(3)	0.1100(2)	4.7(5)
C(6)	0.0522(2)	0.6059(3)	0.0766(1)	3.9(4)
C(7)	0.0970(2)	0.4818(3)	0.0815(1)	3.8(4)
N(3)	0.0923(2)	0.7182(3)	0.0373(1)	5.0(5)
O(2)	0.1735(2)	0.7112(3)	0.0212(1)	7.0(5)
O(3)	0.0455(2)	0.8201(2)	0.0237(1)	6.9(5)
C(8)	0.1587(2)	0.0219(3)	0.1476(2)	4.7(5)
C(9)	0.1321(2)	−0.1081(3)	0.1883(1)	4.0(5)
C(10)	0.1476(2)	−0.0952(3)	0.2677(1)	3.3(4)
C(11)	0.2166(2)	−0.1677(3)	0.3013(2)	4.3(4)
C(12)	0.2308(2)	−0.1497(4)	0.3738(2)	5.1(5)
C(13)	0.1765(2)	−0.0591(3)	0.4107(2)	4.8(5)
C(14)	0.1094(2)	0.0104(3)	0.3745(2)	4.1(4)

Results and discussion

Analytical results and infrared spectroscopy

On the basis of elemental analysis data ('Experimental'), the complex prepared by using the 5NO$_2$-salaep ligand and iron(II) acetate with a 2:1 stoichiometry is formulated as FeL$_2$·MeOH. The complexes prepared either from 5NO$_2$-sal-N(1,4,7,10) or 5NO$_2$-sal-N(1,5,8,12) are formulated as FeL·MeOH while the complex prepared from 5NO$_2$-sal-N(1,5,9,13) is formulated as FeL·0.5MeOH.

TABLE 3. Selected interatomic distances (Å) and bond angles (°) for [Fe(5NO_2-salaep)$_2$] (**1**) with e.s.d.s in parentheses

Iron environment			
Fe–O(1)	2.057(2)	O(1)–Fe–N(2)	168.32(7)
Fe–N(2)	2.225(2)	O(1)–Fe–N(2′)	87.05(8)
Fe–N(1)	2.185(3)	N(1)–Fe–N(1′)	179.21(9)
O(1)–Fe–O(1′)	86.79(8)	N(1)–Fe–N(2)	85.82(8)
O(1)–Fe–N(1)	84.94(8)	N(1)–Fe–N(2′)	93.68(8)
O(1)–Fe–N(1′)	95.64(8)	N(2)–Fe–N(2′)	100.66(8)
Ligand			
O(1)–C(3)	1.276(3)	C(4)–C(5)	1.359(4)
N(1)–C(1)	1.280(3)	C(5)–C(6)	1.398(4)
N(1)–C(8)	1.477(4)	C(6)–C(7)	1.375(4)
N(2)–C(10)	1.343(3)	C(6)–N(3)	1.437(4)
N(2)–C(14)	1.350(3)	C(8)–C(9)	1.521(4)
N(3)–O(2)	1.237(5)	C(9)–C(10)	1.501(4)
N(3)–O(3)	1.232(4)	C(10)–C(11)	1.385(4)
C(1)–C(2)	1.445(4)	C(11)–C(12)	1.378(4)
C(2)–C(3)	1.442(4)	C(12)–C(13)	1.373(4)
C(2)–C(7)	1.395(4)	C(13)–C(14)	1.373(4)
C(3)–C(4)	1.431(4)		
C(3)–O(1)–Fe	126.8(2)	C(5)–C(6)–C(7)	120.9(3)
C(1)–N(1)–Fe	122.3(2)	C(5)–C(6)–N(3)	119.2(3)
C(8)–N(1)–Fe	122.7(2)	C(7)–C(6)–N(3)	119.9(3)
C(1)–N(1)–C(8)	114.5(2)	C(2)–C(7)–C(6)	120.7(2)
C(14)–N(2)–Fe	117.7(2)	C(6)–N(3)–O(2)	118.7(3)
C(10)–N(2)–C(14)	118.0(2)	C(6)–N(3)–O(3)	118.7(3)
C(10)–N(2)–Fe	123.4(2)	N(1)–C(8)–C(9)	112.8(2)
N(1)–C(1)–C(2)	127.5(2)	C(8)–C(9)–C(10)	112.6(2)
C(1)–C(2)–C(3)	123.3(2)	N(2)–C(10)–C(9)	117.0(2)
C(1)–C(2)–C(7)	116.9(2)	N(2)–C(10)–C(11)	121.9(2)
C(3)–C(2)–C(7)	119.8(2)	C(9)–C(10)–C(11)	121.0(2)
O(1)–C(3)–C(2)	123.2(2)	C(10)–C(11)–C(12)	119.5(3)
O(1)–C(3)–C(4)	120.1(2)	C(11)–C(12)–C(13)	118.8(3)
C(2)–C(3)–C(4)	116.7(2)	C(12)–C(13)–C(14)	119.2(3)
C(3)–C(4)–C(5)	122.2(3)	O(2)–N(3)–O(3)	122.5(3)
C(4)–C(5)–C(6)	119.8(3)	N(2)–C(14)–C(13)	122.7(3)

Table 4 lists some pertinent IR frequencies for the isolated ligands and their iron(II) complexes. Comparison of the listed values allows us to conclude that the phenolic oxygen atoms and imine nitrogen atoms are coordinated to the iron(II) atom. We tentatively assign the weak and broad frequency near 500 cm^{-1} which is present in the complexes and lacking in the ligand spectra, to the Fe–O phenolic bond [27, 28] (**1**: 492, **2**: 496; **3**: 503; **4**: 501 cm^{-1}).

On comparing the IR spectra of the iron(II) and manganese(II) [12] complexes including the same ligands, it is interesting to concentrate on the two complexes including the 5NO_2-sal-N(1,4,7,10) ligand where the four nitrogen atoms are linked through 'short' ethylene bridges. Considering the manganese(II) complex, we observe that the ν(NH) stretching frequencies (3323 and 3303 cm^{-1}) are high compared to those of the other complexes in the manganese(II) series and that Δ(C=N) (free ligand–manganese(II) complex) is very small (8 cm^{-1}). On the contrary, the iron(II) complex including the same ligand is characterized by ν(NH) and ν(C=N) stretching frequencies similar to those of the other complexes in the iron(II) series. This apparent discrepancy can be rationalized by considering the difference in ionic radius between the two ions: the 'short' 5NO_2-sal-N(1,4,7,10) hexadentate ligand can more easily wrap around the small Fe^{2+} ion than it does around the larger Mn^{2+} ion which results in M–N bonds stronger with Fe^{2+} compared to Mn^{2+}.

Molecular structure of 1

The unit cell includes four mononuclear [Fe(5NO_2-salaep)$_2$] molecules as shown by the stereoview of Fig. 3. The stacking of the molecules through π interactions involving the salicylaldimine rings of adjacent molecules affords ribbons along the [001] direction. The distance between the planes of the stacked moieties is *c.* 3.8 Å (see 'Supplementary material'). These ribbons are stacked along the [100] direction with a sliding of half the dimension of the *b* parameter of the unit cell. The insertion of two pyridine moieties from a molecule between the two salicylaldimine rings of an adjacent molecule provide the cohesion of the crystal in the [010] direction through van der Waals interactions. The shortest interatomic distances between iron atoms (8.82 and 9.70 Å) are situated between neighbouring ribbons along *a* and *b*, respectively, while the distance between the iron atoms inside a ribbon, i.e. along *c*, is 11.63 Å. The extent of these Fe...Fe separations together with the presence of intercalated bulky ligands and the absence of bridging ligands precludes magnetic exchange interactions between neighbouring Fe(II) ions to operate, as further substantiated in the magnetic susceptibility section.

The [Fe(5NO_2-salaep)$_2$] molecule is comprised of a central iron atom coordinated to two tridentate 5NO_2-salaep ligands affording a distorted coordination octahedron as shown in Fig. 2 and evidenced by the range of Fe–O and Fe–N distances and L–Fe–L angles (Table 3). The distortion of the coordination octahedron lowers considerably the symmetry of the molecule and the *trans* N(1) and N(1′) nitrogen donors can be viewed as apical to a twisted O(1) N(2′) N(2) O(1′) basal plane (see 'Supplementary material'). As a matter of fact, the strain imposed by the tridentate ligand shifts O(1) and N(2) fairly above and O(1′) and N(2′) fairly below the basal plane and the significant difference between the Fe–O(1) and Fe–N(2) bond lengths increases the twisting of this plane. The overall distortion of the coordination octahedron results in a symmetry lower than rhombic.

The 5NO_2-salaep ligands are comprised of two almost perfectly planar parts involving

TABLE 4. Significant IR absorptions[a] of iron(II) complexes **1–4** and uncoordinated ligands

Compound				Assignment
1	**2**	**3**	**4**	
3417	3410	3415	3419	ν(OH)(MeOH)
(~3400)	(~3400)	(~3400)	(~3400)	ν(OH), ν(NH)
	3285	3263	3267	ν(NH)
(1662)	(1652)	(1663)	(1659)	ν(C=N)
1616	1623	1628	1623	ν(C=N)
(1612)	(1611)	(1613)	(1612)	ν(N–O)
1598	1595	1596	1596	ν(N–O)
(1312)	(1320)	(1326)	(1312)	ν(N–O)
1297	1310	1309	1310	ν(N–O)
954	989	981	982	$\nu(CH_2)$
941	973	968	973	$\nu(CH_2)$
904	944	950	946	$\nu(CH_2)$
875	916	916	914	$\nu(CH_2)$
			905	$\nu(CH_2)$
			880	$\nu(CH_2)$
835	832	830	836	ν(CH)ϕ
780				ν(CH)(py)
768				ν(CH)(py)
758				ν(CH)(py)
492	496	503	501	ν(Fe–O) or ν(Fe–N)
386	384	404	403	ν(Fe–O) or ν(Fe–N)
286	315	339	335	ν(Fe–O) or ν(Fe–N)
216	203	234	226	ν(Fe–O) or ν(Fe–N)

[a]Frequencies in cm^{-1}; frequencies in parentheses correspond to free ligands.

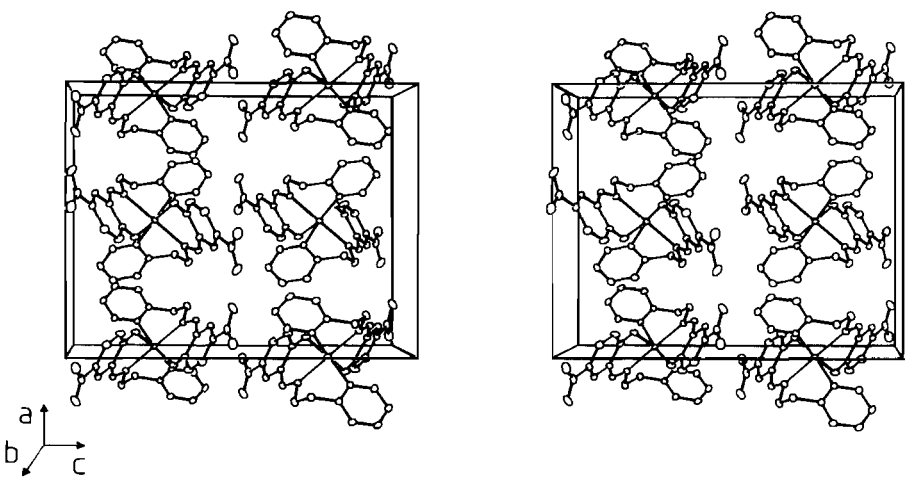

Fig. 3. Stereoview of the unit cell of [Fe(5NO_2-salaep)$_2$] (**1**) along [010].

N(2)–C(10)–C(11)–C(12)–C(13)–C(14)–C(9) and O(1)–C(3)–C(4)–C(5)–C(6)–C(7)–C(2)–C(1)–N(1), respectively. The large folding angle between the two parts of the ligand (113.4°) (see 'Supplementary material') is due to the presence of two electronic delocalization networks extended over the aforementioned sets of atoms, respectively, and separated by the C(8)–C(9) 'insulating' ethylene group. Remarkably, the aforementioned twisting of the O(1) N(2') N(2) O(1') coordination plane results partly from this folding.

Comparison of the iron(II) coordination octahedron of **1** with that of the ferrous ion of the bacterial reaction centers [1c] evidences significant similarities: (i) the ligand environment is comprised of four nitrogen and two oxygen donor atoms in both cases;

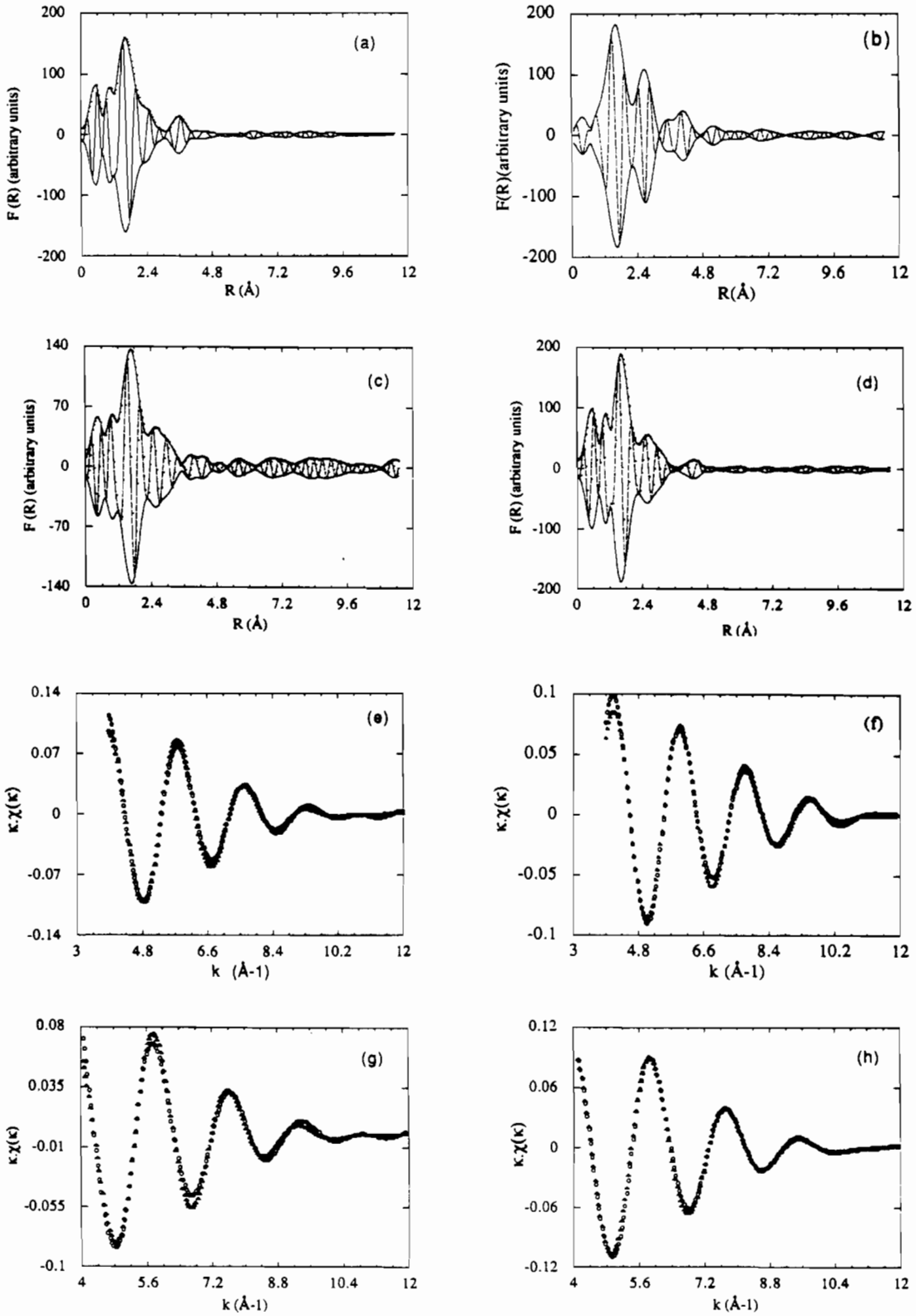

Fig. 4. (a)–(d) Fourier Transforms of the EXAFS spectra of complexes **1–4** at 300 K including the modulus (full line) and imaginary parts (dotted line). (e)–(h) Comparison of the experimental and calculated $k \cdot \chi(k)/k$ values for the first filtered shell of complexes **1–4** (Δ experimental, O calculated).

(ii) the oxygen donor atoms are *cis* to each other in both coordination octahedra and (iii) the distortion of the coordination octahedron of the iron(II) in **1** is very similar to that of the ferrous ion of photosynthetic bacteria as evidenced when comparing Fig. 4 of ref. 1c and Fig. 2 of this work.

X-ray absorption

The X-ray absorption data are displayed in Fig. 4 for the EXAFS, and in Fig. 5 for the edge structures. Distances and Debye–Waller factors for the first shell are gathered in Table 5. Values of the energies and estimates of the intensity of the main features of the edge are displayed in Table 6.

The Fourier transforms of the four spectra are very similar and characteristic of mononuclear complexes, with a large distribution of oxygen and nitrogen neighbours in the first coordination shell. The quantitative analysis of the EXAFS data of the first shell is summarized in Table 5. The second shell of neighbours includes essentially the carbon skeleton of the ligands and is more or less separated from the first one according to the complexes. We did not attempt to analyze this second shell. No significant signal is present at a distance larger than 3.6 Å, in particular no heavy atom contribution, which is in accordance with the mononuclear nature of the complexes. The analysis of the local structure of these four parent compounds is difficult and the conclusions drawn must be considered with caution.

Taking these difficulties into account and to avoid apparently good fits having no physical meaning: (i) we constrained the number of fitted parameters to the mininum (in particular we chose the same values of Γ and E^0 for the two or three subshells of the first shell for each complex and kept the scale factor equal to one); (ii) the experimental results were fitted with various distributions of neighbours

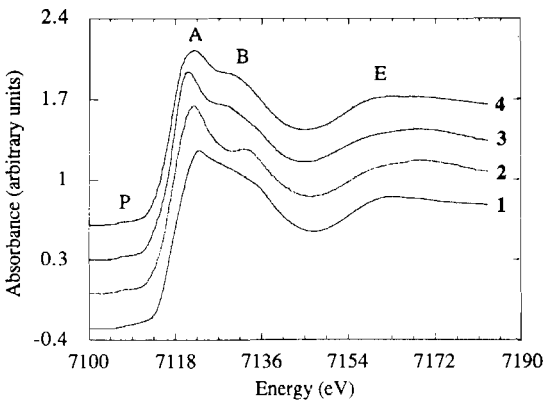

Fig. 5. XANES spectra of complexes **1–4** at 300 K (P: pre-edge; A: top of the edge; B: shoulder; E: first EXAFS oscillation).

TABLE 5. Parameters resulting from the analysis of the first shell EXAFS data

Parameters[a]	Complex			
	1	**2**	**3**	**4**
1st. subshell				
R_1 (Å)	2.04 (2.06)[b]	2.10	2.02	2.02
σ_1 (Å)	0.03	0.05	0.02	0.02
No. and postulated nature of neighbours	2O	2O+2N	2O	2O
2nd. subshell				
R_2 (Å)	2.18 (2.18)[b]	2.24	2.16	2.17
σ_2 (Å)	0.05	0.01	0.05	0.05
No. and postulated nature of neighbours	2N	2N	3N	3N
3rd. subshell				
R_3 (Å)	2.23 (2.23)[b]		2.20	2.21
σ_3 (Å)	0.04		0.02	0.01
No. and postulated nature of neighbours	2N		1N	1N
E° (eV)	7109	7111	7109	7109
Γ	1.5	1.5	1.8	1.5
ρ (%)	1.5	2.1	2.1	0.9

[a]The fitted parameters are: the Fe–neighbour distances R_i, the Debye–Waller factors, σ_i; the ionization energy, E°; the constant Γ used to define the free mean path of the electron: $\lambda = k/\Gamma$. The agreement factor is $\rho = \Sigma_i(\chi^i_{exp} - \chi^i_{cal})^2/(\chi^i_{exp})^2$. [b]From the XRD molecular structure.

(2O+4N, 2O+2N+2N or 2O+3N+1N for example). Since the theoretical amplitude and phase parameters used are very close for oxygen and nitrogen, which have close Z atomic numbers, the agreement factors were very close from each other in some of these attempts. We report therefore in Table 5 the atomic distribution which is the most likely, not only on the basis of the results of the fits but also on the grounds of XRD and/or chemical arguments. For example, concerning complex **1**, we were guided by the XRD results to choose a set of EXAFS determined bond lengths close to the crystallographic ones, among several equally satisfactory fits. Concerning **2**, we report only the values of the fit obtained for one mixed (2O+2N) and one 2N subshells since the calculations involving three subshells (2O+2N+2N) gave no significantly different Fe–O and Fe–N distances.

The metal to ligand separations reported in Table 5 for complexes **1**, **3** and **4** are similar and include: (i) two short distances at 2.03±0.02 Å attributed to Fe–O bonds on the grounds that oxygen has a greater affinity than nitrogen for the iron(II) as

TABLE 6. Energy and relative intensity of the XANES spectra

Complex	Energy (eV) (and relative intensity)			
	Pre-edge (P)	Top of the edge (A)	Shoulder (B)	First EXAFS oscillation (E)
1	7108.3 (vw)[a]	7122.8 (1.56)[b]	7133.0	7163.0
2	7108.0 (vw)	7122.2 (1.64)	7132.3	7169.0
3	7107.4 (vw)	7121.0 (1.63)	7128.0	7168.0
4	7106.9 (vw)	7121.8 (1.52)	7128.0	7162.5

[a]vw: very weak. [b]Absorbance, relative to the atomic absorption taken as unit.

evidenced for example in the XRD structure of **1**; (ii) medium distances at 2.17 ± 0.02 Å (two Fe–N in **1** and three Fe–N in **3** and **4**); (iii) larger distances at 2.22 ± 0.02 Å (two Fe–N in **1** and one Fe–N in **3** and **4**). The differences in Fe–L distances between **1**, **3** and **4** for a given subshell are of the order of magnitude of the accuracy. However, the distances of all three subshells to the metal center are smaller in **1**, which is consistent with the conclusion drawn from the analysis of the Mössbauer data (following section), i.e. the strain exerted by the two tridentate N_2O ligands of **1** is reduced compared to that exerted by the N_4O_2 hexadentate ligand of **3** and **4**.

Concerning the iron(II) complex exhibiting a spin transition, **2**, it is worth noticing that the two shortest distances in the first shell (2Fe–O and 2Fe–N) appear to be very close to each other, with an approximately 2.10 Å value, generating a stronger ligand field than in **1**, **3** and **4**, close enough to the critical ligand field where the spin transition occurs.

The edge spectra of all four complexes are similar and typical of distorted octahedral Fe(II) complexes. The intensity of the pre-edge, which corresponds to a {(1s)2...(3d)6} to {(1s)1...(3d)7} transition is very weak, as expected for complexes with a first coordination sphere having close to an inversion centre, where such transitions are symmetry forbidden. Consequently, the underlying multiplet structure is unresolved, given the weakness of the transition and the experimental resolution (≈ 2 eV or more). Therefore, the pre-edge energy differences observable in Table 6 are not significant since they have been determined on weak, poorly defined features.

The top of the edge, which is afforded by the symmetry allowed {(1s)2...(4p)0} to {(1s)1..(4p)1} transitions, is characterized by an absorbance A which is not large compared to the atomic absorption (from 1.52 in **4** to 1.64 in **2**) and an important width, including the shoulder at higher energy. Both features are at variance with the sharp white line ($A > 2$) observed for $[Fe(H_2O)_6]^{2+}$ where all the Fe–O distances are equivalent in a perfect octahedron. The situation described for complexes **1–4** is usually observed for distorted octahedral complexes, where a large distribution of distances splits the empty p molecular levels. It is also likely that multiple scattering by the carbon atoms of the ligands is also operating in this energy range. As in the case of the EXAFS data, the main differences in the edge spectra are observed for complex **2**, where the two main edge transitions are best resolved and the intensity of the top of the edge is maximum. The first EXAFS oscillation (E) is structured in the four complexes, as could be anticipated from the distribution of the distances evidenced by EXAFS. Small variations in the distances and number of neighbours change rather significantly the position in energy of the first EXAFS oscillation (from ≈ 7163 eV in **1** to 7169 eV in **2**, for example).

Magnetic susceptibility

Complexes **1–4** have been measured as microcrystalline powders at different temperatures. The room temperature data in Table 7 indicate the presence of high-spin iron(II) in **2** and **4**. Complex **4** shows a small decrease of the effective magnetic moment at temperatures below 30 K consistent with the presence of a small zero-field splitting. The μ_B/Fe values obtained from polycrystalline samples of **1** and **3** are given in parentheses in Table 7. These values show that the room temperature magnetic moment of **1** and **3** are slightly higher than those usually observed for high-spin iron(II) species and increase to *c.* 6BM/Fe at 5 K.

This magnetic behavior is thought to arise from alignment of the crystallites in the magnetic field

TABLE 7. Effective magnetic moments of complexes **1–4** at different temperatures

Complex	μ_B/Fe(BM)				
	300 K	97 K	47 K	24 K	5 K
1	5.40 (5.69)	5.39 (5.88)	5.31 (6.09)	5.17 (6.22)	4.67 (6.22)
2	5.30	1.31	1.27	1.24	1.18
3	5.03 (5.38)	4.81 (5.34)	4.79 (5.51)	4.67 (5.76)	4.32 (5.91)
4	5.26	5.20	5.15	5.17	4.99

[29]. In order to assess the origin of this behavior, the magnetic susceptibility of **1** and **3** was also measured on vaseline mulls of the samples. The resulting values (Table 7, figures without parentheses) show a slight lowering of μ_{eff} at all temperatures, such that μ_B/Fe remains constant down to 25 K below which it decreases to 4.67 (**1**) and 4.32 (**3**) BM/Fe. These results confirm the interpretation of the values obtained for the polycrystalline samples of **1** and **3** and are in agreement with the behavior expected for high-spin iron(II) complexes in which there is zero-field splitting of the ground state.

A significant decrease of the magnetization of complex **2** is observed between 200 and 100 K. A detailed magnetic susceptibility temperature dependence study has shown the presence of an unusual two-step high-spin (HS) to low-spin (LS) transition for this complex with occurrence of a spin-state equilibrium at *c.* 50% of HS and LS molecules over a 30 K temperature range [30].

Mössbauer spectroscopy

The Mössbauer spectra for the present series of complexes were obtained between 4.2 K and room temperature. In the case of complexes **1**, **3** and **4**, each spectrum consists of a single quadrupole split doublet. Concerning **2**, the high temperature spectra ($T > 190$ K) consist of a single quadrupole split doublet while the spectra obtained at lower temperature are more complicated. A detailed analysis of the Mössbauer spectra of complex **2** has been given in a preliminary paper [30] and will be briefly discussed later in this section. Each doublet was least-squares fit with two Lorentzian lines, each constrained to have the same area [31].

The isomer shift and quadrupole splitting parameters of these complexes are given in Table 8. The values indicate the presence of high-spin iron(II) centers in all complexes except for the low temperature form of **2** which is low-spin Fe(II) [31, 32].

TABLE 8. Mössbauer data[a] for the bacterial reaction centers, PS 2 particles and complexes **1–4**

Sample	T (K)	δ (mm s^{-1})	ΔE_Q (mm s^{-1})
Bacterial reaction centers [9]	200	1.11	1.84
	80	1.16	2.20
	4.2	1.17	2.22
PS 2 particles [10][b]	200	1.13	2.23
	80	1.18	2.63
	4.2	1.18	2.66
1	200	1.07	2.43
	85	1.11	2.60
	4.2	1.11	2.60
2[c]	200	1.02	2.79
	130	1.04 (0.45)	2.84 (0.96)
	4.2	1.08 (0.45)	3.03 (0.95)
3	200	1.06	2.85
	100	1.09	2.91
	4.2	1.10	2.94
4	200	1.06	3.16
	100	1.10	3.19
	4.2	1.10	3.21

[a]Relative to natural Fe foil. [b]Quadrupole splitting values between 2.2 and 2.9 mm s^{-1} are observed at 4.2 K in various PS 2 preparations, the isomer shift values being, however, similar to those above within experimental uncertainty (V. Petrouleas and B. Diner, unpublished results and ref. 5). [c]Values in parentheses give the low-spin component parameters. The 4.2 K parameters of the high-spin component were determined after trapping a sizeable fraction of this state by rapid freezing from room temperature.

Furthermore, the isomer shift values are entirely consistent with a N_4O_2 ligand set [8].

The quadrupole splitting values show some variation among the complexes but all are relatively large indicating that the T_{2g} orbital triplet is split by crystal field distortions affording lower than octahedral symmetry and that the lower state is an orbital singlet. Thermal population of the two higher orbital states results in the observed temperature variation of the quadrupole splitting [33]. This variation is weak in the present case indicating a rather large splitting of the T_{2g} states. The relatively stronger temperature dependence in complex **1** indicates a smaller separation between the ground state and at least one of the excited orbital states than in complexes **3** and **4**. Comparison with complex **2** is hindered by the thermally induced HS/LS equilibrium operating in this complex.

A comparative examination of the ligand environment of Fe(II) in complexes **1–4** evidences that the strain exerted over the metal–ligand bonds by two N_2O tridentate ligands (**1**) should be less than

that exerted by one N_4O_2 hexadentate ligand (**2–4**). Further evidence along these lines comes from an examination of the spectra at 4.2 K in an applied magnetic field of 8 kOe (Fig. 6) [34]: the splitting/broadening of the spectra is smaller in **1** than in **3** and **4** which is consistent with a smaller orbital state separation in the former complex.

In Table 8, comparison of the Mössbauer parameters is also made with the bacterial reaction centers and photosystem 2 preparations. The similarity of the isomer shift values is consistent with the presence of an N_4O_2 donor set in the photosynthetic bacteria and photosystem 2. Complex **1** shows additional similarities, particularly with photosystem 2 preparations, in the quadrupole splitting values; it also shows a small broadening of the absorption peaks in the presence of a magnetic field at 4.2 K (Fig. 6), similar to that observed in photosynthetic bacteria and photosystem 2 preparations [8, 9]. Apparently the present series of complexes are good candidates for comparison with the photosynthetic Fe(II) and in particular complex **1** is a valid model of the immediate environment of the Fe(II) as already documented in the molecular structure section.

The 100 and 4.2 K Mössbauer spectra of **2** consist of two components, the main doublet (90%) being characterized by parameters attributable to low-spin iron(II) [31, 32] (Table 8) and the outer component (10%) being similar to the high-spin 200 K doublet. In order to determine the fraction of high-spin molecules as a function of temperature, twenty Mössbauer spectra of **2** were obtained in the 200–85 K temperature range. Most spectra consist of two doublets in thermal equilibrium one with the other. At high temperature (>180 K), the spectrum consists exclusively in the outer doublet ($\delta = 1.023$, $\Delta E_Q = 2.792$ mm s^{-1}) characteristic of a high-spin Fe(II) $^5T_{2g}$ state. At lower temperatures, an inner doublet develops at the expense of the outer doublet as the temperature is decreased. At low temperatures (<120 K), the spectrum mainly consists in the inner doublet ($\delta = 0.45$, $\Delta E_Q = 0.96$ mm s^{-1}) characteristic of a low-spin Fe(II) $^1A_{1g}$ component.

The spin-state conversion occurs in two steps separated by a 30 K domain in which a perfect thermal spin-state equilibrium involving *c.* 50% of high-spin and low-spin molecules is retained. Below 120 K, the high-spin fraction does not decrease anymore, indicating that this spin-state equilibrium is characterized by a ~10% residual high-spin fraction at low temperature. Both steps of the spin conversion are fairly abrupt as ~90% of the decrease in x_{HS} observed for the first step occurs within ~7 K while 90% of the decrease in x_{HS} for the second step occurs within 14 K [30].

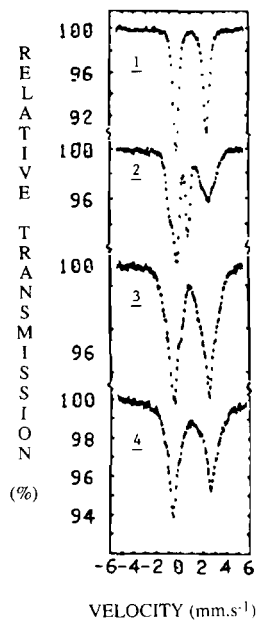

Fig. 6. Mössbauer spectra of complexes **1–4** at 4.2 K in an applied magnetic field of 8 kOe. In the case of complex **2** a large fraction of the high-spin component was trapped by rapid freezing from room temperature.

Conclusions

The infrared data, chemical analysis, X-ray crystal structure, X-ray absorption and Mössbaur spectroscopy and variable temperature magnetic susceptibility study provide evidence that the four compounds described in this study are mononuclear iron(II) complexes. They include either two N_2O tridentate Schiff base ligands (**1**) or one N_4O_2 hexadentate Schiff base ligand (**2–4**) affording more or less distorted octahedral N_4O_2 ligand environments to the iron(II) center.

Among these complexes, **1** exhibits several of the properties required to afford a modelling of the ligand environment of the iron in the 'ferroquinone complex' of bacteria and photosystem 2: (i) high-spin iron(II) center in the 5–300 K temperature range; (ii) ligand environment including two oxygen donor atoms *cis* to each other and four nitrogen donor atoms and affording a distortion of the iron coordination octahedron very similar to that described for the ferrous ion of photosynthetic bacteria; (iii) Mössbauer parameters (isomer shift and quadrupole splitting) similar to those measured for the iron center of the 'ferroquinone complex'; (iv) no observable splitting of the absorption lines of the quadrupole split doublet in an applied magnetic field. These observations and comparison of the results obtained for **1** on the one had and **2–4** on the other hand allow us to confirm that the nature and extent

of the distortion of the Fe(II) coordination octahedron are factors prevailing over the nature of the ligands with regards to the design of spectral analogues of the iron center of the metalloprotein of the 'ferroquinone complex' of photosynthetic bacteria and photosystem 2.

Complex **2** exhibits a thermally induced $^5T_{2g} \leftrightarrow {}^1A_{1g}$ spin conversion with unprecedented features: (i) iron(II) in a ligand environment including four nitrogen and two oxygen donor atoms; (ii) spin conversion of discontinuous nature occurring in two steps separated by a 30 K broad spin equilibrium domain in which *c.* 50% of HS and LS molecules are present.

Supplementary material

Figures 7 and 8 showing the experimental EXAFS spectra before normalization (300 K) and the least-squares fitted Mössbauer spectra (4.2 K) of complexes **1–4**, respectively (3 pages); Tables 9–12 listing crystallographic data, hydrogen atom positional parameters, final non-hydrogen atoms thermal parameters, deviations of atoms from their least-squares planes for complex **1**, respectively (5 pages); Table 13 listing the observed and calculated structure factor amplitudes for complex **1** (14 pages) are available from the authors on request.

Acknowledgements

We thank the Etablissement Public Régional and the CNRS (Action de Recherche Intégrée 'Chimie Biologie' and ATP Photosynthèse) for partial support of this work. The Greek Ministry of Research and Technology and the French Ministère des Affaires Etrangères are gratefully acknowledged for partial support of this work through the Greek–French Scientific Exchange Program.

References

1 (a) J. Deisenhofer, O. Epp, K. Miki, R. Huber and H. Michel, *J. Mol. Biol., 180* (1984) 385; (b) *Nature (London), 318* (1985) 19; (c) H. Michel, O. Epp and J. Deisenhofer, *EMBO J., 5* (1986) 2445; (d) J. P. Allen, G. Feher, T. O. Yeates, D. C. Rees, J. Deisenhofer, H. Michel and R. Huber, *Proc. Natl. Acad. Sci. U.S.A., 83* (1986) 8589; (e) J. P. Allen, G. Feher, T. O. Yeates and D. C. Rees, *Prog. Photosynth. Res., 1* (1987) 375; (f) T. O. Yeates, H. Komiya, A. Chirino, D. C. Rees, J. P. Allen and G. Feher, *Proc. Natl. Acad. Sci. U.S.A., 85* (1988) 7993; (g) J. P. Allen, G. Feher, T. O. Yeates, H. Komiya and D. C. Rees, *Proc. Natl. Acad. Sci. U.S.A., 85* (1988) 8487; (h) H. Komiya, T. O. Yeates, D. C. Rees, J. P. Allen and G. Feher, *Proc. Natl. Acad. Sci. U.S.A., 85* (1988) 9012.

2 (a) B. A. Diner and V. Petrouleas, *Biochim. Biophys. Acta, 1015* (1990) 131; (b) V. Petrouleas and B. A. Diner, *Biochim. Biophys. Acta, 849* (1986) 264.

3 J. L. Zimmerman and A. W. Rutherford, *Biochim. Biophys. Acta, 851* (1986) 416.

4 B. A. Diner and V. Petrouleas, *Biochim. Biophys. Acta, 895* (1987) 138.

5 W. F. Butler, D. C. Johnston, M. Y. Okamura, H. B. Shore and G. Feher, *Biophys. J., 32* (1980) 967.

6 W. F. Butler, R. Calvo, D. R. Fredkin, R. A. Isaakson, M. Y. Okamura and G. Feher, *Biophys. J., 45* (1984) 497.

7 G. C. Dismukes, H. A. Frank, R. Friesner and K. Sauer, *Biochim. Biophys. Acta, 764* (1984) 253.

8 (a) B. Boso, P. Debrunner, M. Y. Okamura and G. Feher, *Biochim. Biophys. acta, 638* (1981) 173; (b) B. Boso, *Ph.D. Thesis,* University of Illinois at Urbana Champaign, 1982.

9 V. Petrouleas and B. A. Diner, *Adv. Photosynth. Res., (Proc. VI Int. Conf. Photosynthesis), I* (1984) 2.195.

10 D. M. Arciero, J. D. Lipscomb, B. H. Huynh, T. A. Kent and E. Münck, *J. Biol. Chem., 258* (1983) 14981.

11 L. Que Jr., J. D. Lipscomb, R. Zimmerman, E. Münck, N. R. Orme-Johnson and W. H. Orme-Johnson, *Biochim. Biophys. Acta, 452* (1976) 320.

12 B. Mabad, P. Cassoux, J. P. Tuchagues and D. N. Hendrickson, *Inorg. Chem., 25* (1986) 1420.

13 N. Rhoda and A. V. Fraioli, *Inorg. Synth., 4* (1953) 159.

14 D. Luneau, J. M. Savariault, P. Cassoux and J. P. Tuchagues, *J. Chem. Soc., Dalton Trans.,* (1988) 1225.

15 B. K. Teo, *EXAFS, Basic Principles and Analysis*, Springer, Berlin, 1986.

16 (a) A. Michalowicz, J. Huet and A. Gaudemer, *Nouv. J. Chim., 6* (1982) 79; (b) M. Verdaguer, A. Michalowicz, J. J. Girerd, N. Alberding and O. Kahn, *Inorg. Chem., 19* (1980) 3271; (c) A. Michalowicz, M. Verdaguer, Y. Mathey and R. Clement, in H. Mandelkow (ed.), *Current Topics in Chemistry,* Vol. 145, Springer, Berlin, 1988, p. 107.

17 A. Michalowicz, in M. Verdaguer and H. Dexpert (eds.), *Structures fines d'absorption en chimie,* Vol. 3, No. 1, Ecole du CNRS, Garchy, 1988.

18 F. James and M. Roos, *MINUIT Program,* a system for function minimization and analysis of the parameters errors and correlations; *Comput. Phys. Commun., 10* (1975) 345.

19 B. K. Teo and P. A. Lee, *J. Am. Chem. Soc., 101* (1979) 2815.

20 A. Mosset, J. J. Bonnet and J. Galy, *Acta Crystallogr., Sect. B, 33* (1977) 2639.

21 B. A. Frentz, *SDP-Structure Determination Package,* Enraf-Nonius, Delft, The Netherlands, 1982.

22 G. M. Sheldrick in G. M. Sheldrick, C. Krüger and R. Goddard (eds.), *Crystallographic Computing 3,* Oxford University Press, London, 1985, p. 175.

23 D. T. Cromer and J. T. Waber, in *International Tables for X-ray Crystallography,* Vol. IV, Kynoch Press, Birmingham, U.K., 1974, pp. 99, 101, Table 2.2.B.

24 D. T. Cromer, in *International Tables for X-ray Crystallography*, Vol. IV, Kynoch Press, Birmingham, U.K., 1974, p. 149, Table 2.3.1.
25 G. M. Sheldrick, *SHELX 76, program for crystal structure determination, University of Cambridge, Cambridge, U.K., 1976.*
26 C. K. Johnson, *ORTEP, Rep. ORNL-1794*, Oak Ridge National Laboratory, Oak Ridge, TN, 1965.
27 K. Nakamoto, *Infrared and Raman Spectra of Inorganic and Coordination Compounds*, Wiley, New York, 3rd edn., 1978, p. 207.
28 J. R. Ferraro, *Low Frequency Vibrations of Inorganic and Coordination Compounds*, Plenum, New York, 1971.
29 B. J. Kennedy and K. S. Murray, *Inorg. Chem., 24* (1985) 1552 and refs. therein.
30 V. Petrouleas and J. P. Tuchagues, *Chem. Phys. Lett., 137* (1987) 21.
31 N. N. Greenwood and T. C. Gibb, *Mössbauer Spectroscopy*, Chapman and Hall, London, 1972, Ch. 6.
32 P. Gutlich and U. Gonser (eds.), *Mössbauer Spectroscopy*, Springer, New York, 1975, Ch. 2.
33 R. Ingalls, *Phys. Rev. A, 133* (1964) 787.
34 V. Petrouleas, B. A. Diner, A. S. Rakotonandrasana and J. P. Tuchagues, *Recl. Trav. Chim. Pays-Bas (Proc. 3rd. Int. Conf. Bioinorg. Chem.), 106* (1987) 220.